

# Machine Learning S-wave Scattering Phase Shifts Bypassing the Radial Schrödinger Equation

Alessandro Romualdi\* and Gionni Marchetti†  
(Dated: April 5, 2022)

We present a machine learning model resting on convolutional neural network (CNN) capable to yield accurate scattering phase shifts in s-wave caused by different three-dimensional spherically symmetric potentials at fixed collision energy thereby bypassing the radial Schrödinger equation. We obtain good performance even in the presence of potential instances supporting bound states.

Phase shifts play a key role in partial wave analysis, and are the crucial quantities for obtaining the scattering amplitude by which the elastic scattering properties of the physical or chemical system of interest can be calculated<sup>1</sup>. In particular, phase shifts  $\delta_0$  in s-wave, i.e., when the angular momentum number  $l = 0$ , are significant for atomic collisions in ultracold regime where the s-wave scattering channel dominates<sup>2–4</sup>. Moreover, in Coulomb systems the s-wave phase shift allows the  $\delta_l$  with  $l = 1, 2, \dots$  to be recursively determined starting from the knowledge of  $\delta_0$ <sup>5</sup>. Therefore the need of accurate computations of the phase shifts in physics, chemistry and materials science can hardly be overemphasized. In this regard, Kohn developed one of the most used method for accurately computing the phase shifts based on the variational principle and the Schrödinger equation<sup>1,6,7</sup>, and very recently a new method and new code, based on a recurrence relation and the variable phase method (VPM)<sup>8–11</sup>, respectively, aiming at the same task have been put forward<sup>5,12</sup>. Despite the fact that solving the one-dimensional radial Schrödinger equation for a given regular potential  $V^{\text{sc}}$  may be a not so difficult task once one chooses the suitable integration algorithm for the problem at hand, it would be highly desirable to provide a supervised machine learning (ML) approach as a *proof of concept*.

In fact, the universal approximation theorem for the neural networks<sup>13</sup> suggests that the continuous mapping between the scattering potential and phase shift can be learned by means of a feed-forward convolutional neural network (CNN)<sup>14,15</sup>, similar to that successfully used in image recognition tasks<sup>16–21</sup>.

Thus, following the recent success in the applying machine learning to physics, chemistry and materials science<sup>22–24</sup>, e.g., accurate predictions of the quantities such as the molecular ground state energy<sup>25,26</sup>, polarizability<sup>27</sup>, atomization energy<sup>28</sup>, density of states at Fermi energy of crystalline solids<sup>29</sup>, identification of the phases of matter<sup>30–32</sup>, development of ML potentials<sup>33–37</sup> and construction of deep-learning wavefunctions of the electronic Schrödinger equation<sup>38,39</sup>, we herein propose a supervised machine learning approach resting on CNN for yielding accurate phase shifts bypassing the radial Schrödinger equation.

Our model is capable of predicting the target phase shifts in s-wave, caused by different three-dimensional spherically symmetric regular potentials at fixed collision

energy with relative error much less than 1%, and corresponding ML accuracy in terms of the average of the mean absolute percentage error (MAPE)  $\lesssim 0.1\%$ . This is remarkable, considering that the approximate phase shifts computed in the first Born approximation and the exact ones are considered to agree very well when the relative error is  $\lesssim 5\%$ <sup>1</sup>.

More importantly, our paper clearly shows the crucial role played by the descriptor (or fingerprint)<sup>40–42</sup> that needs to be physically motivated in order to guarantee a good ML’s performance. In the present case the Hamiltonian is  $H = T + V^{\text{sc}}$ , where  $T, V^{\text{sc}}$  are the kinetic energy and the scattering potential, respectively. Thus, at a given kinetic energy for which the phase shifts in s-wave need to be determined, the potential  $V^{\text{sc}}$  uniquely determines the Hamiltonian. This situation is analogous to that of the Coulomb Matrix (CM) descriptor<sup>28,43</sup> that is constructed on the external potential as the latter determines the molecular Hamiltonian uniquely<sup>44</sup>. Thus, according to the “featureless” approach proposed by Mills et al.<sup>45</sup> each instance of  $V^{\text{sc}}$  can be represented by a suitable image  $X$  thus providing a meaningful descriptor for the nonrelativistic scattering problem, see Section I C for details.

Our work shows that CNN’s regression task becomes difficult whenever a data set corresponding to a given scattering potential contains a number of potential’s instances supporting bound states. We argue that these instances hinder the CNN’s learning task of the phase function  $r \mapsto \delta_0(r)$  where  $r$  is the interparticle distance, for this function takes a step-like form in accordance with the Levinson’s theorem<sup>9,46</sup>.

Note that throughout this paper the computations were performed assuming the typical scattering units, that is,  $\hbar = 2m = 1$ ,  $m$  being the reduced mass of the scattering particle. Therefore in such units  $k, k^2$  are the wave number and energy of the scattering particle in the center of mass reference frame, respectively.

## I. METHODS

### A. Three-Dimensional Spherically Symmetric Potentials

In order to address the problem of learning quantum scattering phase shifts from data, we consider three-

dimensional spherically symmetric potentials that satisfy some nice mathematical properties in accordance with the scattering theory. In particular, the latter requires the scattering potentials to be reasonable smooth functions of the interparticle distance and to fall off sufficiently fast in the asymptotic region<sup>9</sup>.

In the present work our choice of the potentials was dictated by their theoretical and practical importance in various branches of physics and chemical physics. In the following we briefly list the potentials under scrutiny.

The Thomas-Fermi (TF) potential (or Yukawa potential)  $V^{\text{TF}}$  accounts for the screened Coulomb interaction and the strong interaction in condensed matter systems<sup>47–49</sup> and nuclear and particle physics<sup>50</sup>, respectively. In its attractive form this potential has the following expression  $V^{\text{TF}}(r) = -V_0^{\text{TF}} \exp(-qr)/r$  where the positive quantities  $r, q, V_0^{\text{TF}}$  denote the interparticle distance, the screening parameter and the potential's strength, respectively.

A linear combination of the TF potentials gives rise to a scattering potential of significant importance in nuclear and condensed matter physics<sup>51,52</sup>. Here we shall consider a double Yukawa (DY) potential  $V^{\text{DY}}$  which is just a linear combination of two TF potentials, i.e.  $V^{\text{DY}}(r) = V_{01} \exp(-q_1 r)/r + V_{02} \exp(-q_2 r)/r$ . In this paper we shall tune the parameters  $q, V_{01}, V_{02}$  in such a way that it will be repulsive and attractive at short and long distances, respectively<sup>9</sup>, see Section IC for details.

In plasma physics the screened Coulomb interaction is often accounted for by means of the exponential cosine (EC) screened Coulomb potential  $V^{\text{EC}}(r) = V_0^{\text{EC}} \exp(-qr) \cos(qr)/r$ <sup>53–59</sup>. Note that both potentials  $V^{\text{EC}}$  and  $V^{\text{TF}}$  derive directly from the random phase approximation (RPA), thus neglecting the short-range exchange and correlation effects in electronic systems<sup>49</sup>.

Finally, our study will include the square-well (SW) potential  $V^{\text{SW}}$  that plays a fundamental role in the modeling of short-range interactions in various physical systems. In particular, the SW potential is useful as first approximation to the nuclear interaction between a neutron and a proton in a deuteron<sup>60</sup>. The attractive  $V^{\text{SW}}$  is defined by<sup>61</sup>

$$V^{\text{SW}} = \begin{cases} -V_0, & r \leq a \\ 0, & r > a \end{cases} \quad (1)$$

where the positive quantities  $V_0, a$  defines the SW potential's depth and radius, respectively. For a given collision energy  $k^2$ , the phase shift  $\delta_0$  is given by<sup>61</sup>

$$\tan \delta_0 = \frac{k j'_0(ka) j_0(\alpha a) - \alpha j_0(ka) j'_0(\alpha a)}{k n'_0(ka) j_0(\alpha a) - \alpha n_0(ka) j'_0(\alpha a)}, \quad (2)$$

where the prime denotes differentiation with respect to the function's argument, and  $\alpha^2 = k^2 + V_0$ . Here the symbols  $j_0, n_0$  denote the spherical Bessel functions. Note that Eq. 2 is beset by modulo  $\pi$  ambiguity, i.e.  $\delta_0$  is defined up to addition of an arbitrary multiple of  $\pi$ <sup>62,63</sup>.

## B. Computation of the Quantum Phase Shifts: The Variable Phase Approach

The standard computation of the phase shifts takes place in two stages. First, given a spherically symmetric regular potential  $V^{\text{sc}}(r)$ , one needs to solve the following radial Schrödinger equation

$$u_l''(r) + [k^2 - V^{\text{cf}}(r) - V^{\text{sc}}(r)] u_l(r) = 0, \quad (3)$$

for  $u_l(r)$  with the initial condition  $u_l(0) = 0$  at the origin for a given angular momentum number  $l$  ( $l = 0, 1, \dots$ ). The repulsive centrifugal potential  $V^{\text{cf}}(r) = l(l+1)/r^2$  vanishes in our case as we shall limit ourselves to the computation of the s-wave phase shift  $\delta_0$  only. Therefore Eq. 3 in s-wave becomes

$$u_0''(r) + [k^2 - V^{\text{sc}}(r)] u_0(r) = 0. \quad (4)$$

The solution  $u_0$  can be obtained by numerically integrating Eq. 4. Note that this task requires the knowledge of the range of  $V^{\text{sc}}$  in order to avoid possible inaccuracies and round-off errors as well. Finally, the quantity  $\delta_0$  is obtained by matching the numerical solution with the free solution of Eq. 4 in the asymptotic region, i.e., where the effects of  $V^{\text{sc}}$  are negligible. As a consequence one needs to solve an algebraic equation for  $\delta_0$  of the same kind of Eq. 2, thereby involving the spherical Bessel functions  $j_0, n_0$ , and their corresponding derivatives. In general, the above approach is cumbersome.

An alternative approach to the computation of the phase shifts is given by the variable phase method<sup>8–10,64</sup>. Despite the fact that the VPM follows from a simple mathematical property, that is, a homogeneous second order differential equation such as the radial Schrödinger equation can be reduced to a first order nonlinear equation of Riccati type, it really presents a paradigmatic shift in the partial wave analysis as the phase shifts are no longer regarded as mere scalar quantities. In fact, not only the VPM yields the value of the phase shift directly, but promotes it from a scalar quantity to a phase function  $r \mapsto \delta_0(r)$ , so providing important physical insights about the collision effects due to the presence of a particular potential<sup>9</sup>.

The variable phase method rests on the following differential equation for the function  $\delta_0(r)$

$$\delta'_0(r) = -\frac{V^{\text{sc}}(r)}{k} \left[ \cos \delta_0(r) \hat{j}_0(kr) - \sin \delta_0(r) \hat{n}_0(kr) \right]^2, \quad (5)$$

with the boundary condition at the origin  $\delta_0(0) = 0$ . In Eq. 5 the symbols  $\hat{j}_0, \hat{n}_0$  denote the Riccati-Bessel functions.

The numerical integration of Eq. 5 yields the value of  $\delta_0$  directly by taking the asymptotic limit of the solution, i.e.  $\lim_{r \rightarrow \infty} \delta_0(r) = \delta_0$ <sup>9,65</sup>. Moreover, the VPM automatically removes the modulo  $\pi$  ambiguity<sup>9,65,66</sup>. The latter property gives the following expression for the Levinson's

theorem<sup>9,46</sup>

$$\lim_{k \rightarrow 0} \delta_0(k) = n_0 \pi, \quad (6)$$

where  $n_0$  is the number of bound states that the scattering potential is capable to form in s-wave at low energy.

In Fig. 1 the phase shift  $\delta_0$  as function of  $r$  due to the presence of an attractive TF potential with  $V_0^{\text{TF}} = 5$ ,  $q = 1.1$  obtained by means of the VPM for  $k = 0.1$  is shown. It is evident that after an abrupt change the phase function  $\delta_0(r)$  converges to  $\delta_0 \approx \pi$  in the asymptotic region. Therefore, according to Levinson's theorem, see Eq. 6, this TF potential's instance support one bound state in s-wave, and therefore the respective phase function takes a typical step-like behaviour<sup>9,67</sup> as displayed in Fig. 1. However, the information about the presence of one or more bound states can be completely lost, at level of the phase function, when the collision energy is increased. This fact is illustrated in Fig. 1 by the plot of the phase function curve corresponding to the above TF potential's instance but obtained at  $k = 10$ . In the same figure the phase function curves corresponding to the EC and DY potentials with  $V_0^{\text{EC}} = 5$ ,  $q = 1.8$  and  $V_{02} = 2V_{01} = 20$ ,  $q_2 = 2q_1 = 2.0$ , computed at  $k = 0.1$  and  $k = 0.5$ , respectively, are displayed. All the curves in Fig. 1, see also Table I for details, correspond to scattering potentials' instances chosen at random according to the parameters contained in the data sets on which the CNN are trained. They clearly exemplify the different learning tasks that the CNN have to undertake in order to approximate  $r \mapsto \delta_0(r)$  at a given collision energy, i.e.  $k^2$ , for the  $V^{\text{sc}}$ 's instance of interest.

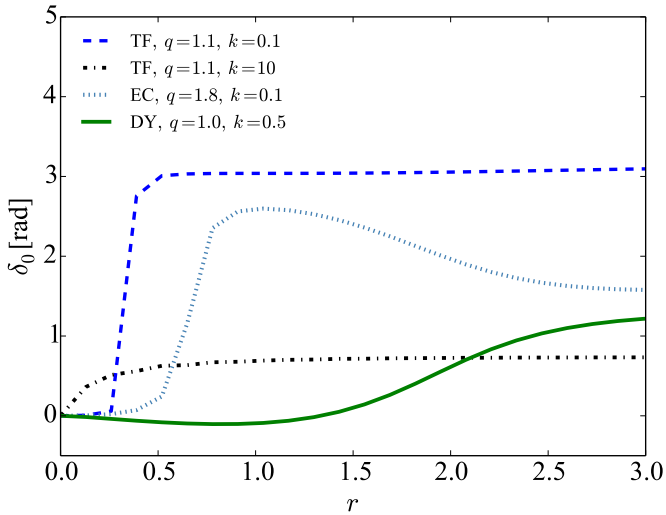


FIG. 1. The phase shift  $\delta_0$  as function of  $r$  caused by the TF, EC, DY potentials' instances chosen at random from the data sets, computed by means of the VPM for different values of  $k$  and  $q$  of interest. We refer the reader to Table I for all the information about the potentials' parameters and the corresponding asymptotic values of  $\delta_0$ .

TABLE I. The strengths and screening parameters of the TF, EC, DY potentials along with the respective phase shifts computed by means of VPM at different values of  $k$  are shown, respectively. Note that  $V_{02} = 2V_{01} = 20$  and  $q_2 = 2q_1 = 2.0$  for the DY potential.

$V^{\text{sc}}$	parameters	$k$	$\delta_0$
$V^{\text{TF}}$	$V_0^{\text{TF}} = 5, q = 1.1$	0.1	3.15
$V^{\text{TF}}$	$V_0^{\text{TF}} = 5, q = 1.1$	10	0.73
$V^{\text{EC}}$	$V_0^{\text{EC}} = 5, q = 1.8$	0.1	1.61
$V^{\text{DY}}$	$V_{01} = 10, q_1 = 1.0$	0.5	1.28

### C. Image of the Scattering Potential Instance as Suitable Descriptor

Given a scattering potential  $V^{\text{sc}}$ 's instance in our ML model, the corresponding descriptor is an image  $X$  of dimension  $N$  pixels, i.e.  $N$  is the resolution of the image, such that it contains the values for the potential's instance evaluated at  $N$  different points of a discretized support interval  $I_s = [r_0, r_1, r_2, \dots, r_N]$ , i.e.  $X = [V(r_0), V(r_1), V(r_2), \dots, V(r_N)]$ . The minimum  $r_0$  and the maximum  $r_N$  of the set  $I_s$  are chosen according to the typical behaviour of the potential  $V$  under scrutiny in the neighborhood of the origin and its asymptotic regime, respectively. Thus, for a fixed strength of  $V^{\text{sc}}$  the resolution  $N$  would determine a coarse-grained view of such a potential, thereby causing the image's details to vary smoothly with the screening parameter  $q$ . In Fig. 2 six images  $X$  corresponding to different instances of  $V^{\text{DY}}$  with parameters  $V_{01} = 10$ ,  $V_{02} = 20$  and  $q_1 \equiv q$ ,  $q_2 = 2q$ ,  $q$  being in  $[1, 2]$  such that it is repulsive a short distance and attractive in the asymptotic region, are shown. Our proposed descriptor offers a good compromise between the accuracy and the computation time.

However, it is not possible to apply such a representation to the potential  $V^{\text{SW}}$  as its image on the discretized interval  $I_s$  would not always encode small variations with respect to the screening parameter  $a$ . To overcome this issue we shall resort to the effective range approximation<sup>60,68</sup> that holds for small values of  $k$  only, see Section II for details.

Finally, it is worth noting that the statistical learning performed by the CNN will be done assuming that each scattering potential's strength is fixed. The reason is that the phase shift  $\delta_0$  caused by an instance of the same potential but with a different strength can be directly derived by an appropriate scaling<sup>9</sup>.

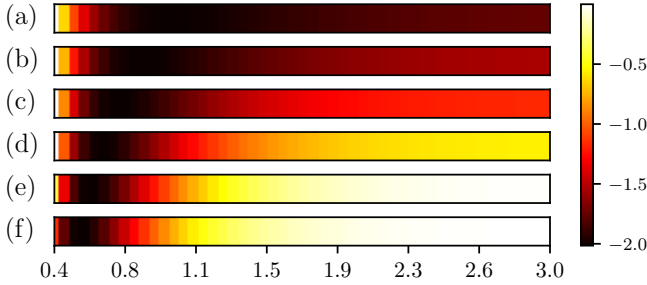


FIG. 2. The images  $X$  labelled by (a), (b), (c), (d), (e), (f) relative to the scattering potential  $V^{\text{DY}}$  with  $V_{01} = 10, V_{02} = 20$  and  $q_1 \equiv q, q_2 = 2q$  obtained for  $q = 1.0, 1.2, 1.42, 1.62, 1.8, 1.99$ , respectively. The color (pixel intensity) indicates the value of the potential.

#### D. Data Sets

For each scattering potential, except the SW potential, a data set  $D_k = \{(X_1, \delta_0^{(1)}), (X_2, \delta_0^{(2)}), \dots, (X_n, \delta_0^{(n)})\}$  where  $n = 1000$  is constructed for  $k = 0.1, 0.5, 5, 10$ , respectively. Each image descriptor  $X_\mu$  is labelled by the corresponding phase shift  $\delta_0^{(\mu)}$  computed at fixed wave number  $k$  by means of the VPM whose implementation rests on the algorithm LSODA<sup>12,69</sup>. We divide each data set  $D_k$  into training, validation and test sets. The CNN's learning is performed within the training set, while the validation set is used to adjust the model hyperparameters by studying the model convergence during the learning phase. Finally, the assessment of the CNN's accuracy is performed on the test set.

The TF and EC potentials' parameters upon which the respective data set  $D_k$  are constructed are  $V_0^{\text{TF}} = V_0^{\text{EC}} = 5$  and  $q$  being uniformly generated in  $[0.5, 2.5]$  and  $[0.5, 2]$ , respectively. According to this choice of parameters some instances of TF potential can form bound states in s-wave, while none instance of EC potential cannot support them. In this regard, we estimated that roughly 30% instances of TF potentials in  $D_{0.1}$  can form one bound state.

The parameters of interest for the DY potential were introduced in Section 1B. In the latter case the screening parameter values were uniformly chosen at random in  $[1, 2]$ . None of the DY potential's instances is capable of forming bound states.

Finally, two data sets of shallow SW potentials with depth  $V_0 = 0.25$  and radii  $a$  uniformly chosen in  $[0.4, 2]$  are generated computing the respective s-wave phase shifts according to Eq. 2 at  $k = 0.01, 0.1$ .

#### E. Convolutional Neural Network

Our model is composed of a linear stack of  $L = 5$  one-dimensional convolutional layers each followed by a

max-pooling layer. In each convolutional layer different numbers of filters, each of size 3 pixels, take the output of the previous layer (or the input image in case of the first layer) and extract features while scanning 1 pixel at time. Each convolution is followed by the Rectified Linear Unit (ReLU) activation. In this way, the computation units of a convolutional layer create feature maps that summarise the presence of relevant details in the input images.

After each convolution layer, a max-pooling layer summarizes the most activated output of the feature map, resulting in a down sampled representation of the layer input. As the information is processed through the layers of the network, convolutional and max-pooling operations make the model able to capture patterns of progressively higher complexity. Hence the number of filters in each layer are progressively increased to allow for more abstraction. In particular, we used 64, 128, 256, 256, 256 filters on the first to the last convolutional layer, respectively. At the end of the network a series or two fully connected layers, the first one with output size 1024, and the last one with a single output, perform label prediction based on the features extracted by the last max-pooling layer. The CNN have been implemented on TensorFlow<sup>70</sup> (version 2.4.0), and trained by means of the Adam optimizer<sup>71</sup>.

## II. RESULTS AND DISCUSSION

In order to assess the CNN's performance over the above data sets we adopt two estimator measures: the mean square error (MSE) and mean absolute percentage error. First, we train the CNN by minimizing the MSE during the training phase using the Adam optimizer. Second, we report the MAPE between the true and predicted phase shifts in the test set as a measure of model performance. Note that unless differently specified, the training happened over 100 epochs on 16 mini batch using a learning rate of  $1 \times 10^{-4}$ .

In panels (a), (b), (c), (d) of Fig. 3, Fig. 4 and Fig. 5 the scatter plots of the prediction versus the reference s-wave phase shift caused by TF, DY, and EC, respectively, at  $k = 0.1, 0.5, 5, 10$  are shown. For all these potentials the MAPE is comparable and varies from 0.01% to 0.03% when the learning occurs for  $k = 0.5, 5, 10$ . There is a plausible physical explanation of these similar learning performance obtained despite the different functional form of the scattering potentials under study. The reason is that increasing the energy for the screening parameters under scrutiny each scattering potential affects the phase function in the neighbourhood of the origin only. To understand this, one just needs to look at the scatter plot relative to DY potential in panels (c) and (d), Fig. 4 where the phase shifts are negative. This happens because the repulsive part of the DY potentials' instances mainly affect the phase function nearby the origin as a consequence to our choice of the screening parameters. On the other hand, by inspections of some instances of

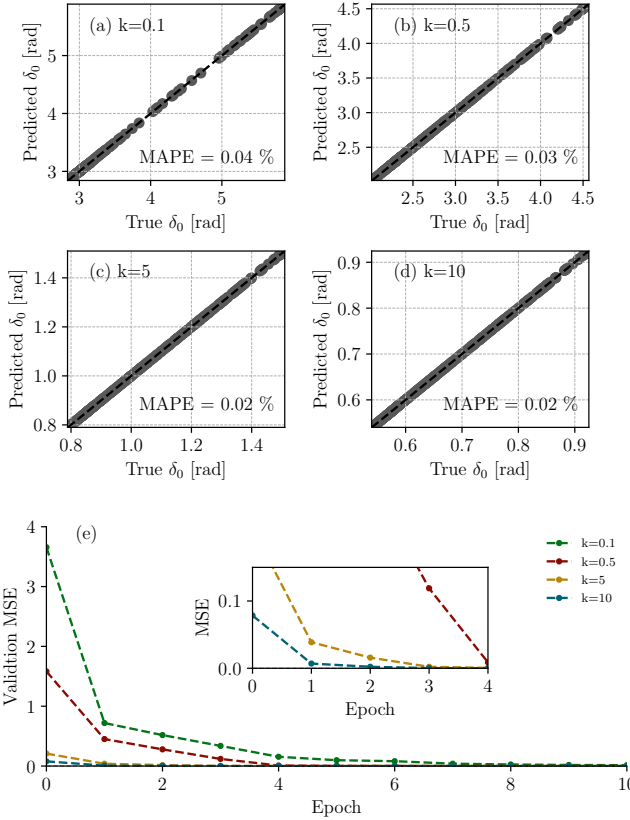


FIG. 3. In panels (a), (b), (c), (d) predictions versus reference phase shifts  $\delta_0$  caused by the TF potential at  $k = 0.1, 0.5, 5, 10$ , respectively, are shown. Panel (e) displays the relative learning curves as functions of the training epochs. The inset shows the earlier convergence achieved when  $k = 5, 10$ .

the TF, DY, and EC potentials' data sets we found that for the parameters of interest, increasing the energy the phase function  $r \mapsto \delta_0(r)$  takes a smooth form for each  $V^{\text{sc}}$ . For instance, this smooth behaviour is illustrated by the plot of the phase function due to a TF potential's instance at  $k = 10$  in Fig. 1. Thus, the CNN's learning task become easier at higher collision energies, that is, increasing  $k$ . On the other hand this observation is confirmed looking at the learning curves as functions of epochs shown in panel (e) of Fig. 3, Fig. 4 and Fig. 5 for  $k = 5, 10$  where a far smaller number of epochs with respect to that observed for  $k = 0.1$  is necessary for achieving the convergence.

On the contrary, the Adam optimizer algorithm takes considerably more epochs to converge over the data set corresponding to small values of  $k$ . This change of learning rate is particularly evident  $k = 0.1$ . The latter increasing learning difficulty can be understood if for example we look at the data set  $D_{0.1}$  corresponding to  $V^{\text{TF}}$ . In such a case we know that it contains about 30% in-

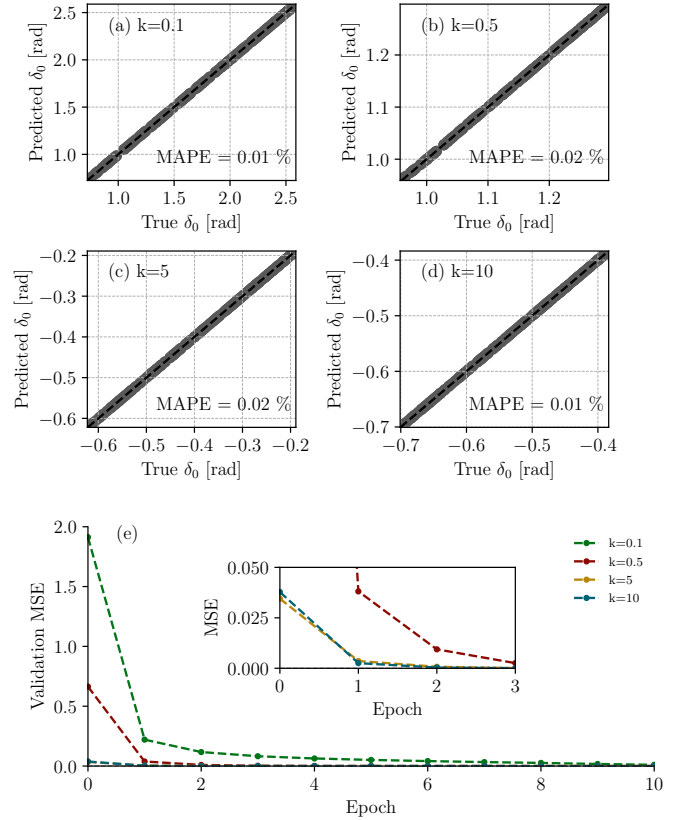


FIG. 4. In panels (a), (b), (c), (d) predictions versus reference phase shifts  $\delta_0$  caused by the DY potential at  $k = 0.1, 0.5, 5, 10$ , respectively, are shown. Panel (e) displays the relative learning curves as functions of the training epochs. The inset shows the earlier convergence achieved when  $k = 5, 10$ .

stances supporting one bound state in s-wave. Therefore the CNN's prediction of the s-wave phase shifts for the  $V^{\text{TF}}$  now requires to approximate a phase function presenting an abrupt change due to the emergence of plateau in correspondence of  $\delta_0 \approx \pi$  as explained in Section (see also Fig. 1). On the other hand, the phase functions relative to  $V^{\text{EC}}$  and  $V^{\text{DY}}$  certainly exhibit a far richer functional form at low energy as illustrated by two respective phase functions chosen at random in Fig. 1.

Moreover, we note that the CNN perform similarly on the data sets corresponding to TF and EC potentials across all the values of  $k$  under scrutiny. Curiously, the latter potentials are an approximation of the very same effective RPA potential. However, the learning goal of the DY potential when  $k = 0.1$  proves much more difficult yielding a MAPE of 0.16%.

Overall, despite some difficulties shown by the learning curves at low energies our ML model yields accurate predictions of the phase shifts caused by TF, EC, DY potentials whose relative error is much less than 1%.

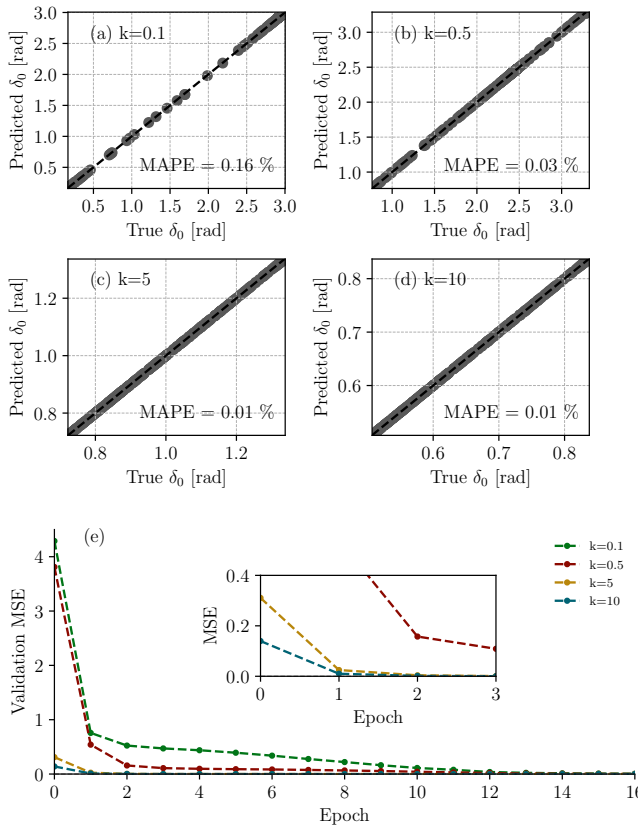


FIG. 5. In panels (a), (b), (c), (d) predictions versus reference phase shifts  $\delta_0$  caused by the DY potential at  $k = 0.1, 0.5, 5, 10$ , respectively, are shown. Panel (e) displays the relative learning curves as functions of the training epochs. The inset shows the earlier convergence achieved when  $k = 5, 10$ .

As explained in Section IC it is not possible to meaningfully represent the SW potential as an image as proposed in our approach. To overcome this issue, we can resort the effective range approximation for short-range potentials<sup>60,68</sup> that is applicable in s-wave scattering at low energy, i.e.  $k \approx 0$ . This approximation reads as<sup>68</sup>

$$k \cot \delta_0 \approx -\frac{1}{c_0} + \frac{1}{2} k^2 r_0, \quad (7)$$

where  $c_0, r_0$  are called the scattering length and the effective range, respectively. In general, for simple potentials such as the SW and TF potentials,  $\delta_0$  depends only on the depth and range of the scattering potential under study<sup>61</sup>. From Eq. 7 it is then possible to fix the TF potential's parameters  $V_0^{\text{TF}}, q$  in terms of  $V_0, a$  relative to the SW potential, so that the former yields the same s-wave shifts  $\delta_0$  caused by the SW potential and hence computed according to Eq. 2. This approach is often called the shape independent approximation. In this regard, one needs to compute  $c_0, r_0$  for both potentials, and then compare them.

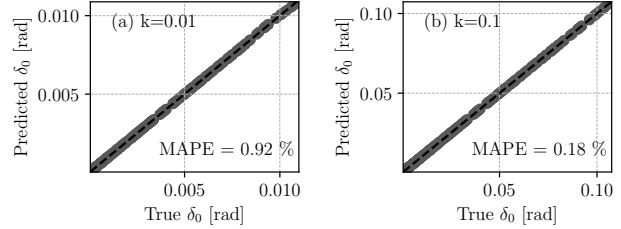


FIG. 6. In panels (a), (b) predictions versus reference phase shifts  $\delta_0$  caused by the SW potential replaced by the TF potential according to the scattering length approximation (Eq. 7) at  $k = 0.01, 0.1$ , respectively, are shown.

Therefore, one finds that the image of a SW potential can be successfully replaced by that of a TF potential whose parameters are given in terms of those of the SW potential as  $V_0^{\text{TF}} = (1/3)(5/2)^{3/2} V_0, q = (5/2)^{1/2} a^{-1}$ .

In panels (a), (b) of Fig. 6 the scatter plots of the prediction versus the reference s-wave phase shift according to the effective range approximation applied to the SW potential<sup>72</sup>, at  $k = 0.01, 0.1$ , respectively, are shown. As MAPE are 0.92%, 0.18%, for  $k = 0.01, 0.1$  respectively, this scattering approximation combined with our ML model yield satisfactory accurate predictions of the phase shifts  $\delta_0$ .

Our analysis suggests that our ML model is effectively learning the phase functions after being trained on the scattering potential images  $X_\mu$  labelled by the respective phase shift  $\delta_0^{(\mu)}$ .

### III. CONCLUSION

We presented a novel machine learning model that can accurately predict the phase shifts in s-wave due to the presence of different regular potentials. More importantly, it effectively proves to be able in learning the phase function  $r \mapsto \delta_0(r)$  at a given collision energy after training on the scattering potential images labelled by the respective reference phase shifts. This task is achieved bypassing the radial radial Schrödinger equation thanks to a physically-motivated descriptor based on the Hamiltonian of the nonrelativistic scattering problem at hand.

Next task could be to construct a model able to predict  $\delta_l$  with  $l = 1, 2, \dots$  a fixed scattering energy by including the centrifugal potential contribution into the descriptor in similar fashion. However, a more ambitious goal would be to effectively learning  $r \mapsto \delta_l(r, k)$  having the wave number  $k$  as additional input.

## ACKNOWLEDGMENTS

AR and GM contributed equally to this study. We thank professor Ravi Rau for pointing out important works regarding the phase amplitude equation.

---

\* alessandro.romualdi@yahoo.com  
 † gionnimirchetti@gmail.com

- <sup>1</sup> C. J. Joachain, *Quantum Collision Theory* (North-Holland, 1975).
- <sup>2</sup> E. Fermi, *Ric. Scientifica* **7** (1936).
- <sup>3</sup> K. Huang and C. N. Yang, *Phys. Rev.* **105**, 767 (1957).
- <sup>4</sup> Z. Idziaszek and T. Calarco, *Phys. Rev. Lett.* **96**, 013201 (2006).
- <sup>5</sup> J.-C. Pain, *Journal of Physics Communications* **2**, 025015 (2018).
- <sup>6</sup> W. Kohn, *Phys. Rev.* **74**, 1763 (1948).
- <sup>7</sup> R. K. Nesbet, *Phys. Rev.* **175**, 134 (1968).
- <sup>8</sup> F. Calogero, *Il Nuovo Cimento (1955-1965)* **27**, 261 (1963).
- <sup>9</sup> F. Calogero, *Variable Phase Approach to Potential Scattering* (Academic Press, 1967).
- <sup>10</sup> V. V. Babikov, *Soviet Physics Uspekhi* **10**, 271 (1967).
- <sup>11</sup> U. Fano and A. R. P. Rau, *Atomic Collisions and Spectra* (Academic Press, Inc., Orlando, Florida, 1986).
- <sup>12</sup> A. Palov and G. Balint-Kurti, *Computer Physics Communications* **263**, 107895 (2021).
- <sup>13</sup> D. Yarotsky, *CoRR* **abs/1804.10306** (2018), arXiv:1804.10306.
- <sup>14</sup> D. Hubel and T. N. Wiesel, *J Physiol.* **160**, 106 (1962).
- <sup>15</sup> K. Fukushima, *Biological Cybernetics* **36**, 193–202 (1980).
- <sup>16</sup> Y. Lecun, L. Bottou, Y. Bengio, and P. Haffner, *Proceedings of the IEEE* **86**, 2278 (1998).
- <sup>17</sup> A. Krizhevsky, I. Sutskever, and G. E. Hinton, in *Advances in Neural Information Processing Systems*, Vol. 25, edited by F. Pereira, C. J. C. Burges, L. Bottou, and K. Q. Weinberger (Curran Associates, Inc., 2012) pp. 1097–1105.
- <sup>18</sup> C. Szegedy, Wei Liu, Yangqing Jia, P. Sermanet, S. Reed, D. Anguelov, D. Erhan, V. Vanhoucke, and A. Rabinovich, in *2015 IEEE Conference on Computer Vision and Pattern Recognition (CVPR)* (2015) pp. 1–9.
- <sup>19</sup> D. Silver, A. Huang, C. J. Maddison, A. Guez, L. Sifre, G. van den Driessche, J. Schrittwieser, I. Antonoglou, V. Panneershelvam, M. Lanctot, S. Dieleman, D. Grewe, J. Nham, N. Kalchbrenner, I. Sutskever, T. Lillicrap, M. Leach, K. Kavukcuoglu, T. Graepel, and D. Hassabis, *Nature* **529**, 489 (2016).
- <sup>20</sup> S. Mallat, *Philosophical Transactions of the Royal Society A: Mathematical, Physical and Engineering Sciences* **374**, 20150203 (2016).
- <sup>21</sup> H. W. Lin, M. Tegmark, and D. Maddison, *Rolnick, Journal of Statistical Physics* **168**, 1223 (2017).
- <sup>22</sup> L. Zdeborová, *Nature Physics* **13**, 420 (2016).
- <sup>23</sup> G. Carleo, I. Cirac, K. Cranmer, L. Daudet, M. Schuld, N. Tishby, L. Vogt-Maranto, and L. Zdeborová, *Rev. Mod. Phys.* **91**, 045002 (2019).
- <sup>24</sup> J. Schmidt, M. R. G. Marques, and M. A. L. Botti, *Silvana. Marques, npj Computational Materials* **5**, 489 (2016).
- <sup>25</sup> F. A. Faber, L. Hutchison, B. Huang, J. Gilmer, S. S. Schoenholz, G. E. Dahl, O. Vinyals, S. Kearnes, P. F. Riley, and O. A. von Lilienfeld, *Journal of Chemical Theory and Computation* **13**, 5255–5264 (2017).
- <sup>26</sup> A. P. Bartók, S. De, C. Poelking, N. Bernstein, J. R. Kermode, G. Csányi, and M. Ceriotti, *Sci Adv.* **3**, e1701816 (2017).
- <sup>27</sup> G. Montavon, M. Rupp, V. Gobre, A. Vazquez-Mayagoitia, K. Hansen, A. Tkatchenko, K.-R. Müller, and O. A. von Lilienfeld, *New Journal of Physics* **15**, 095003 (2013).
- <sup>28</sup> M. Rupp, A. Tkatchenko, K.-R. Müller, and O. A. von Lilienfeld, *Phys. Rev. Lett.* **108**, 058301 (2012).
- <sup>29</sup> K. T. Schütt, H. Glawe, F. Brockherde, A. Sanna, K. R. Müller, and E. K. U. Gross, *Phys. Rev. B* **89**, 205118 (2014).
- <sup>30</sup> L. Wang, *Phys. Rev. B* **94**, 195105 (2016).
- <sup>31</sup> J. Carrasquilla, R. Melko, *Nature Phys* **13**, 431–434 (2017).
- <sup>32</sup> E. van Nieuwenburg, E. Bairey, and G. Refael, *Phys. Rev. B* **98**, 060301 (2018).
- <sup>33</sup> J. Behler and M. Parrinello, *Phys. Rev. Lett.* **98**, 146401 (2007).
- <sup>34</sup> A. P. Bartók, M. C. Payne, R. Kondor, and G. Csányi, *Phys. Rev. Lett.* **104**, 136403 (2010).
- <sup>35</sup> A. P. Thompson, L. P. Swiler, C. R. Trott, S. M. Foiles, and G. J. Tucker, *Journal of Computational Physics* **285**, 316 (2015).
- <sup>36</sup> A. V. Shapeev, *Multiscale Modeling & Simulation* **14**, 1153 (2016).
- <sup>37</sup> J. Behler, *The Journal of Chemical Physics* **145**, 170901 (2016), <https://doi.org/10.1063/1.4966192>.
- <sup>38</sup> J. Hermann, Z. Schätzle, and F. Noé, *Nature Chemistry* **12**, 891 (2020).
- <sup>39</sup> S. Manzhos, *Machine Learning: Science and Technology* **1**, 013002 (2020).
- <sup>40</sup> L. M. Ghiringhelli, J. Vybiral, S. V. Levchenko, C. Draxl, and M. Scheffler, *Phys. Rev. Lett.* **114**, 105503 (2015).
- <sup>41</sup> A. P. Bartók, R. Kondor, and G. Csányi, *Phys. Rev. B* **87**, 184115 (2013).
- <sup>42</sup> K. Rossi and J. Cumby, *International Journal of Quantum Chemistry* **120**, e26151 (2020).
- <sup>43</sup> O. A. von Lilienfeld, *International Journal of Quantum Chemistry* **113**, 1676 (2013).
- <sup>44</sup> P. Hohenberg and W. Kohn, *Phys. Rev.* **136**, B864 (1964).
- <sup>45</sup> K. Mills, M. Spanner, and I. Tamblyn, *Phys. Rev. A* **97** (2018).
- <sup>46</sup> N. Levinson, *Kgl. Danske Videnskab.Selskab., Mat.fys. Medd.* **25** (1949).
- <sup>47</sup> N. W. Ashcroft and M. D. Mermin, *Solid State Physics* (Saunders College, Philadelphia, 1976).
- <sup>48</sup> J. R. Meyer and F. J. Bartoli, *Phys. Rev. B* **23**, 5413 (1981).
- <sup>49</sup> G. Giuliani and G. Vignale, *Quantum Theory of Electron Liquid* (Cambridge University Press, Cambridge, UK, 2005).
- <sup>50</sup> B. Pohv, K. Rith, C. Scholz, and F. Zetsche, *Particles and Nuclei*, 1st ed. (Springer, Berlin, 2002).

<sup>51</sup> N. F. Bali, S.-Y. Chu, R. W. Haymaker, and C.-I. Tan, Phys. Rev. **161**, 1450 (1967).

<sup>52</sup> I. Nagy and B. Apagyi, Phys. Rev. A **58**, R1653 (1998).

<sup>53</sup> C. S. Lam and Y. P. Varshni, Phys. Rev. A **6**, 1391 (1972).

<sup>54</sup> P. K. Shukla and B. Eliasson, Physics Letters A **372**, 2897 (2008).

<sup>55</sup> P. K. Shukla and B. Eliasson, Phys. Rev. Lett. **108**, 165007 (2012).

<sup>56</sup> Lin, C. Y. and Ho, Y. K., Eur. Phys. J. D **57**, 21 (2010).

<sup>57</sup> Z. Moldabekov, T. Schoof, P. Ludwig, M. Bonitz, and T. Ramazanov, Physics of Plasmas **22**, 102104 (2015).

<sup>58</sup> Y. Y. Qi, J. G. Wang, and R. K. Janev, Physics of Plasmas **23**, 073302 (2016).

<sup>59</sup> D. Munjal, P. Silotia, and V. Prasad, Physics of Plasmas **24**, 122118 (2017).

<sup>60</sup> K. S. Krane, *Introductory Nuclear Physics* (John Wiley and Sons, U.S.A, 1988).

<sup>61</sup> A. Z. Capri, *Nonrelativistic Quantum Mechanics*, 3rd ed. (World Scientific, Singapore, 2002).

<sup>62</sup> J. R. Taylor, *Scattering Theory: The Quantum Theory of Nonrelativistic Collisions* (John Wiley & Sons, Inc., New York, 1972).

<sup>63</sup> P. H. E. Meijer and J. L. Repace, American Journal of Physics **43**, 428 (1975).

<sup>64</sup> P. M. Morse and W. P. Allis, Phys. Rev. **44**, 269 (1933).

<sup>65</sup> G. Marchetti, Journal of Applied Physics **126**, 045713 (2019).

<sup>66</sup> K. Chadan, R. Kobayashi, and T. Kobayashi, Journal of Mathematical Physics **42**, 4031 (2001).

<sup>67</sup> M. Portnoi and I. Galbraith, Solid State Communications **103**, 325 (1997).

<sup>68</sup> H. A. Bethe, Phys. Rev. **76**, 38 (1949).

<sup>69</sup> L. Petzold, SIAM Journal on Scientific and Statistical Computing **4**, 136 (1983).

<sup>70</sup> M. Abadi, P. Barham, J. Chen, Z. Chen, A. Davis, J. Dean, M. Devin, S. Ghemawat, G. Irving, M. Isard, M. Kudlur, J. Levenberg, R. Monga, S. Moore, D. G. Murray, B. Steiner, P. Tucker, V. Vasudevan, P. Warden, M. Wicke, Y. Yu, and X. Zheng, in *Proceedings of the 12th USENIX Conference on Operating Systems Design and Implementation*, OSDI'16 (USENIX Association, USA, 2016) p. 265–283.

<sup>71</sup> D. P. Kingma and J. Ba, “Adam: A method for stochastic optimization,” (2014).

<sup>72</sup> Note that in this case, using the same model hyperparameters as in the previous cases, resulted in higher variability in validation loss during training. We regularized the model by reducing the learning rate of the Adam optimizer to  $10^{-6}$  and increasing the training epochs increased to 5000.